

A FIRST LOOK AT CREATING MOCK CATALOGS WITH MACHINE LEARNING TECHNIQUES

XIAOYING XU¹, SHIRLEY HO¹, HY TRAC¹, JEFF SCHNEIDER^{1,2}, BARNABAS POZOS², MICHELLE NTAMPAKA¹

Draft version September 25, 2018

ABSTRACT

We investigate machine learning (ML) techniques for predicting the number of galaxies (N_{gal}) that occupy a halo, given the halo’s properties. These types of mappings are crucial for constructing the mock galaxy catalogs necessary for analyses of large-scale structure. The ML techniques proposed here distinguish themselves from traditional halo occupation distribution (HOD) modeling as they do not assume a prescribed relationship between halo properties and N_{gal} . In addition, our ML approaches are only dependent on parent halo properties (like HOD methods), which are advantageous over subhalo-based approaches as identifying subhalos correctly is difficult. We test 2 algorithms: support vector machines (SVM) and k-nearest-neighbour (kNN) regression. We take galaxies and halos from the Millennium simulation and predict N_{gal} by training our algorithms on the following 6 halo properties: number of particles, M_{200} , σ_v , v_{max} , half-mass radius and spin. For Millennium, our predicted N_{gal} values have a mean-squared-error (MSE) of ~ 0.16 for both SVM and kNN. Our predictions match the overall distribution of halos reasonably well and the galaxy correlation function at large scales to $\sim 5 - 10\%$. In addition, we demonstrate a feature selection algorithm to isolate the halo parameters that are most predictive, a useful technique for understanding the mapping between halo properties and N_{gal} . Lastly, we investigate these ML-based approaches in making mock catalogs for different galaxy subpopulations (e.g. blue, red, high M_{star} , low M_{star}). Given its non-parametric nature as well as its powerful predictive and feature selection capabilities, machine learning offers an interesting alternative for creating mock catalogs.

Subject headings: methods:numerical, galaxies:halos, cosmology:large-scale structure of universe

1. INTRODUCTION

As we enter the era of large-scale structure experiments such as LSST, WFIRST and Euclid, the creation of reliable mock galaxy catalogs will become increasingly more important. Such catalogs are essential for correctly characterizing the expected errors in the analyses of these datasets, calibrating analysis pipelines and ultimately measuring cosmological parameters (such as the dark energy equation of state) from galaxy clustering (e.g. Anderson et al. 2012). Making mock catalogs for different subpopulations of galaxies (e.g. blue versus red, high M_{star} versus low M_{star} , etc.) to study their clustering properties is also of utmost importance for understanding galaxy formation and evolution (e.g. Coil et al. 2008; Guo et al. 2012). Although these mock catalogs can be generated relatively quickly using perturbation theory-based approaches such as that described in Manera et al. (2013), it is well known that these approximations break down at small scales (e.g. Carlson, White & Padmanabhan 2009).

Alternatively, mock catalogs can be created using simulations which capture non-linear structure growth to smaller scales, and inherently include redshift-space distortions (velocity information of the dark matter particles is known). Ideally we would like large-volume cosmological simulations with both N-body and hydrodynamics, however, such simulations are computationally expensive. Hence, the large number of mocks neces-

sary for obtaining robust error measurements renders this approach impractical. Fortunately, since pure N-body simulations are relatively inexpensive, the literature has been rife with methods for populating the dark matter halos found in these simulations with galaxies. One of the most popular methods for doing this is using halo occupation distributions (HODs) which is an analytic model for determining the number of galaxies (N_{gal}) that should form in a halo given its properties (e.g. Zheng et al. 2009). More recently, subhalo abundance matching (SHAM) has become very prevalent (e.g. Conroy, Wechsler & Kravtsov 2007; Vimal et al. 2010). This method relies on being able to correctly identify the subhalos within a halo, a very difficult problem in its own right due to resolution limitations (see e.g. Behroozi, Wechsler & Wu 2011). It then assumes that each subhalo contains a single galaxy with a stellar mass or luminosity that is monotonically related to a subhalo property.

While both methods have been shown to produce mock galaxy catalogs that match observations reasonably well, it would be progressive to attempt to eliminate the above mentioned assumptions. The sophisticated non-parametric regression algorithms that form a subcategory of “machine learning” (ML) are ideal for this purpose. To obtain the mapping from halos to N_{gal} , the only assumptions that these model-independent algorithms require are that such a relationship exists and that it is a continuous function of the halo parameters. They then proceed to construct a model from the data itself and hence do not impose any pre-supposed relationships onto the data. We note that although ML algorithms are non-parametric in the sense that we do not need to

¹ McWilliams Center for Cosmology, Department of Physics, Carnegie Mellon University, 5000 Forbes Ave., Pittsburgh, PA 15213

² School of Computer Science, Carnegie Mellon University, 5000 Forbes Ave., Pittsburgh, PA 15213

assume a known relationship between data parameters, they do often require us to assume some operational parameters such as how severely poor predictions are penalized. These, however, can be optimized as described in §3.1.

In addition, the ML-based approaches we propose here, like HOD-based methods, rely only on the properties of the parent dark matter halo. Hence, we can circumvent the difficulties in subhalo identification. Another point worth highlighting is that in principle, these techniques can be trivially extended to understand how halo properties map onto different subpopulations of galaxies. This provides a method for making mock catalogs for these different subpopulations as well.

ML algorithms do, however, need to be trained on large, accurate datasets in order for them to learn robust mappings between halo properties and galaxy properties such as N_{gal} : a large-volume N-body plus hydro simulation with reliable galaxy formation would be ideal. At present, we have not been able to acquire such a simulation and so we use the Millennium simulation with semi-analytic galaxy formation for this study. However, it is conceivable that such a simulation will become available in the near future which can be used to characterize the halo-galaxy mapping via the ML techniques discussed in this work.

A final point of interest rests in the observation that most HOD methods typically use the halo mass as the only parameter in their halo-to-galaxy mappings. An important topic to study is the sensitivity of N_{gal} to other halo parameters. For example, there have been investigations hinting that the environment of the halo is also an important factor in determining how many galaxies will form (e.g. Gao et al. 2005; Croft et al. 2012). This information can be gleaned using ML techniques as well, through performing a “feature selection” which picks out the halo properties that best predict N_{gal} .

In § 2 we describe the dataset we use derived from the Millennium simulations. In § 3 we describe the 2 ML techniques we employ to learn the mapping between halo properties and N_{gal} . In § 4 we describe our results, i.e. how well our predictions match the actual values from Millennium. This section also includes a discussion on using ML to make mocks for different subpopulations of galaxies. We conclude in § 5.

2. DATASET

We construct our dataset from halo and galaxy catalogs at $z = 0$ derived from the Millennium simulation (Springel 2005; Springel et al. 2005). These catalogs are obtained via querying the Millennium online database (Lemson et al. 2006). The halo catalogs were generated using a friends-of-friends (FoF) algorithm with linking length of 0.2 and the semi-analytic galaxy prescription used to populate these halos is described in Croton et al. (2006); De Lucia et al. (2006); De Lucia & Blaizot (2007). The Millennium simulation is run with 2160^3 particles in a $500h^{-1}\text{Mpc}$ box. The cosmology employed has $\Omega_m = 0.25$, $\Omega_b = 0.045$, $\Omega_\Lambda = 0.75$, $h = 0.73$, $n_s = 1$ and $\sigma_8 = 0.9$.

To obtain our dataset, we search through the Millennium halo catalog and extract all primary halos (FoF groups) with mass greater than $10^{12}h^{-1}M_\odot$ (at present,

we are unlikely to observe anything less massive except in the local Universe). We then match galaxies from the semi-analytic catalog to these halos, keeping only the primary galaxies of a halo or subhalo (i.e. those flagged 0 or 1 in the Millennium database). Hence, we emerge with a halo catalog listing the following 7 parameters: number of particles in the halo N_p , M_{200} , velocity dispersion σ_v , maximum circular velocity v_{max} , half-mass radius $R_{1/2}$, spin and number of galaxies in the halo N_{gal} . Our goal is to train a machine learning algorithm to predict N_{gal} using the other 6 halo parameters.

The semi-analytic model used to populate the Millennium halos with galaxies is dependent on various thresholds (such as for gas accretion and star formation) that are also evolved through time. This quality makes Millennium an adequate testing ground for ML applications because the mapping from halo parameters to N_{gal} is much more complicated than the straight-forward functions normally employed in methods such as HOD and SHAM. The complexity of these mappings should be closer to the level we expect from actual N-body simulations with hydrodynamics.

There are 395,832 halos (with 445,983 total galaxies) in our sample which we use for our basic tests of the ML algorithms. However, since the Millennium semi-analytic model provides b, v, r, i, z magnitudes and stellar masses for the galaxies, we can also use these same halos to learn the mapping between halo properties and N_{gal} for different subpopulations of galaxies. We perform tests of the ML algorithms after splitting the halo sample on colour and stellar mass (a proxy for luminosity) in §4.1 and §4.2 respectively.

3. MACHINE LEARNING ALGORITHMS

We test 2 different machine learning (ML) algorithms for predicting N_{gal} from the halo parameters N_p , M_{200} , σ_v , v_{max} , $R_{1/2}$ and spin. The first is a support vector machine (SVM) and the second is a k-nearest-neighbours (kNN) routine, both described below. They work by “learning” a relationship between a set of input features \mathbf{X} and the value we’re interested in predicting Y . SVM and kNN are both non-parametric in the sense that we do not need to assume a model as traditional methods for populating halos with galaxies do. The mapping is constructed using information in the data itself: the data picks the model best suited to it. In addition, we avoid the messy problem of subhalo finding which is a required step in any SHAM-based approach; like HOD-based models, our proposed ML techniques operate on the parent halo itself.

The learning process is accomplished by “training” the algorithm on a set of training data where Y is known. The learned mapping can then be applied to a test set of \mathbf{X} values with known Y to verify its accuracy. If the learned relationship appears robust, it can be applied to a set of \mathbf{X} with unknown Y to make predictions.

In testing the accuracy of the predicted values, we draw on the mean-squared-error (MSE) defined as

$$\text{MSE} = \frac{\sum_{i=1}^N (Y_{i,\text{test,true}} - Y_{i,\text{test,predicted}})^2}{N} \quad (1)$$

where N is the number of test data points. This effectively measures a combination of variance (the scatter in

the predicted values) and bias (how different from truth the predicted values are).

3.1. Support Vector Machines

Support Vector Machines (SVMs) work by mapping the features \mathbf{X} to a higher dimensional-space and attempting to separate them into regions that map onto specific Y values using a set of hyperplanes (Cortes & Vapnik 1995). In its original form, it is a classification scheme but can be generalized to a regression algorithm (Drucker et al. 1997).

The general idea behind SVM is best illustrated through the case of a binary classifier. The binary SVM is trained on a set of input features $\mathbf{X} = \{X_1, X_2, X_3 \dots X_d\}$, where d is the total number of features, to classify data into one of two classes $Y = \{-1, 1\}$. Consider a set of N training data, each with a corresponding column vector of features \mathbf{X}_i and a corresponding class $Y_i(\mathbf{X}_i) = \pm 1$. An SVM attempts to separate the training data into their appropriate classes using 2 parallel hyperplanes in a high-dimensional space. These planes can be written as

$$\mathbf{W} \cdot \mathbf{X} - b = \pm 1 \quad (2)$$

where \mathbf{W} is the normal vector to the hyperplane and b is some constant scalar analogous to a y -intercept in 2D. The 2 planes must satisfy the condition that no points fall in between them, i.e.

$$\mathbf{W} \cdot \mathbf{X}_i - b \geq 1 \quad (3)$$

for \mathbf{X}_i of the first class (i.e. $Y(\mathbf{X}_i)=1$) or

$$\mathbf{W} \cdot \mathbf{X}_i - b \leq -1 \quad (4)$$

for \mathbf{X}_i of the second class. Note that this can be simply re-written as

$$Y_i(\mathbf{W} \cdot \mathbf{X}_i - b) \geq 1. \quad (5)$$

The region bounded by these 2 planes is known as the margin, which has width

$$w = \frac{2}{\|\mathbf{W}\|}. \quad (6)$$

The best classifier is obtained through maximizing this distance or minimizing $\|\mathbf{W}\|$ subject to the constraint in Equation (5) since in this limit we will obtain the most robust separation of the datapoints. For computational purposes, we actually end up minimizing $\frac{1}{2}\|\mathbf{W}\|^2$. The optimization can be performed using Lagrange multipliers (α_i). This leads to minimizing $\|\mathbf{W}\|$ with respect to the Lagrangian

$$L(\alpha_i) = \frac{1}{2}\|\mathbf{W}\|^2 - \sum_{i=1}^N \alpha_i [y_i(\mathbf{W} \cdot \mathbf{X}_i - b) - 1] \quad (7)$$

subject to the constraints $\alpha_i \geq 0$. Taking the derivative of this Lagrangian with respect to $\|\mathbf{W}\|$ yields the solution

$$\|\mathbf{W}\| = \sum_{i=1}^N \alpha_i Y_i \mathbf{X}_i. \quad (8)$$

Values for the α_i can be obtained by substituting this solution back into Equation (7) which yields

$$L(\alpha_i) = \sum_{i=1}^N \alpha_i - \frac{1}{2} \sum_{i=1}^N \sum_{j=1}^N \alpha_i \alpha_j Y_i Y_j \mathbf{X}_i \cdot \mathbf{X}_j. \quad (9)$$

and maximizing $L(\alpha_i)$ with respect to the α_i . It turns out that only a few of the α_i are non-zero. These correspond to the training points that satisfy the equality condition in Equation (5). Such points are called the support vectors and set the value of b , i.e. ($b = \mathbf{W} \cdot \mathbf{X}_i - Y_i$). In practice, b is taken to be an average over the support vectors, that is

$$b = \frac{1}{N_{SV}} \sum_{i=1}^{N_{SV}} (\mathbf{W} \cdot \mathbf{X}_i - Y_i) \quad (10)$$

where N_{SV} is the number of support vectors.

It is often useful to introduce some slack (quantified by ξ_i below) into the SVM classifier. This amounts to replacing the constraint in Equation (5) with the new constraint

$$Y_i(\mathbf{W} \cdot \mathbf{X}_i - b) \geq 1 - \xi_i. \quad (11)$$

The effective reduction of the margin width in the above equation allows for some misclassification of the data. We then minimize

$$\frac{1}{2}\|\mathbf{W}\|^2 + C \sum_{i=1}^N \xi_i \quad (12)$$

where C is a parameter that determines the penalty for any misclassification. If we solve the Lagrangian for this case, we will find that $\xi_i = \alpha_i/C$ is required.

In addition, one can see that Equation (9) contains the term $\mathbf{X}_i \cdot \mathbf{X}_j$ which is just the dot product between two vectors in feature space. We can then imagine generalizing this dot product to the dot product in a space spanned by a non-linear mapping (Φ) of the features (Aizerman, Braverman & Rozonoer 1964; Boser, Guyon & Vapnik 1992). This mapping can be used to take the features into a higher dimensional space, making them more easily separable. The dot product $\Phi(\mathbf{X}_i) \cdot \Phi(\mathbf{X}_j)$ can be thought of as a kernel function $k(\mathbf{X}_i, \mathbf{X}_j)$. Commonly used kernels like the polynomial, Gaussian (or radial basis function, rbf) and sigmoid functions are popular due to their simplicity. These have the forms

$$k_{poly}(\mathbf{X}_i, \mathbf{X}_j) = (\mathbf{X}_i \cdot \mathbf{X}_j)^m \quad (13)$$

where m is the degree of the polynomial,

$$k_{rbf}(\mathbf{X}_i, \mathbf{X}_j) = \exp(-\gamma \|\mathbf{X}_i - \mathbf{X}_j\|^2) \quad (14)$$

and

$$k_{sigmoid}(\mathbf{X}_i, \mathbf{X}_j) = \tanh(\mathbf{X}_i \cdot \mathbf{X}_j + r), \quad (15)$$

where γ and r are parameters of the kernel.

The simple binary SVM described above can be generalized to support vector regression (SVR) (Drucker et al. 1997) which is the algorithm we employ in this study. For the regression problem, we seek hyperplanes satisfying the equations

$$Y_i - (\mathbf{W} \cdot \mathbf{X}_i - b) \leq \epsilon + \xi_i \quad (16)$$

$$(\mathbf{W} \cdot \mathbf{X}_i - b) - Y_i \leq \epsilon + \xi_i^* \quad (17)$$

Here, ϵ is a tolerance parameter, i.e. there is no penalty assigned to predictions that fall within ϵ of the true value. $\xi_i > 0$ and $\xi_i^* > 0$ are slack variables corresponding to upper and lower constraints on the system output.

The quantity the SVR must minimize is

$$\frac{1}{2} \|\mathbf{W}\|^2 + C \sum_{i=1}^N (\xi_i + \xi_i^*). \quad (18)$$

which closely resembles Equation (12). The Lagrangian takes the form

$$\begin{aligned} L(\alpha_i, \alpha_i^*) = & \frac{1}{2} \|\mathbf{W}\|^2 + C \sum_{i=1}^N (\xi_i + \xi_i^*) \\ & - \sum_{i=1}^N \alpha_i [\epsilon + \xi_i - y_i + (\mathbf{W} \cdot \mathbf{X}_i + b)] \\ & - \sum_{i=1}^N \alpha_i^* [\epsilon + \xi_i^* + y_i - (\mathbf{W} \cdot \mathbf{X}_i + b)] \end{aligned} \quad (19)$$

where α_i and α_i^* are Lagrange multipliers subject to the constraints $0 \leq \alpha_i \leq C$, $0 \leq \alpha_i^* \leq C$ and $\sum_{i=1}^N (\alpha_i - \alpha_i^*) = 0$.

For our analysis, we use the SVR algorithm implemented in the scikit-learn Python library (Pedregosa et al. 2011). We use the default $\epsilon = 0.1$ and find that changing this value does not make a noticeable difference in our predictions or the resulting MSE. The algorithm takes in a value for the penalty parameter C from Equation (18) and the kernel. m , γ and r need also be specified depending on what kernel is being used. Optimal parameter values can be determined by splitting our sample of halos into three equal parts: a training set, a validation set and a test set. We can then train the SVM using some pre-determined grid values: $C = \{100, \dots, 10^9\}$ and γ or $r = \{0.1, \dots, 10^{-8}\}$ in powers of 10, and calculate the MSE of the validation set. The parameter values that give the minimum MSE are chosen for our analyses, where we evaluate how well the ML predictions match truth using the test set.

3.2. *k*-Nearest-Neighbours

The *k*-Nearest-Neighbours (kNN) algorithm is much simpler than the SVM to understand and can also be used for both classification and regression. The kNN routine calculates “distances” to the *k* nearest training data points for each point \mathbf{X}_i that we are interested in predicting Y_i . This distance is often just a simple Euclidean distance between the features \mathbf{X} , however, one can imagine using other definitions as well. The predicted Y_i is then just the average of the *k* nearest training set Y values. This average can be weighted according to distance such that points further away have less impact on the predicted value. Mathematically, one can represent this as

$$Y_i = \frac{\sum_k w(d(\mathbf{X}_k, \mathbf{X}_i)) Y_k}{k} \quad (20)$$

where $d(\mathbf{X}_k, \mathbf{X}_i)$ is the distance between \mathbf{X}_i and one of its *k* nearest neighbours \mathbf{X}_k , and $w(d)$ is the weight corresponding to that distance.

We again use the scikit-learn implementation of kNN (Pedregosa et al. 2011). The algorithm takes in a value for *k*. Again, the optimal value can be found by stepping through a pre-determined set $k = \{3, 6, \dots, 21, 24\}$

and picking the value with the lowest MSE when the algorithm is applied to the validation set.

3.3. Feature Selection

Feature selection is the process by which we select which features are the most relevant for predicting Y from \mathbf{X} . A simple approach to this is forward feature selection which relies on an initial comparison to the base MSE, or the MSE calculated by taking all $Y_{i,test,predicted} = \langle Y_{train} \rangle$ in Equation (1), i.e.

$$\text{Base MSE} = \frac{\sum_{i=1}^N (Y_{i,test,true} - \langle Y_{train} \rangle)^2}{N} \quad (21)$$

This is just the MSE one would obtain by doing the most naive thing: predicting all Y values to be the mean Y of the training set (denoted as $\langle Y_{train} \rangle$ above).

Forward feature selection starts by training an ML algorithm to predict Y using only a single feature. We repeat this for each individual feature and calculate its MSE value from a test set. If the minimum MSE is less than the base MSE, then we are doing better than the naive prediction, indicating that the features do contain information that is correlated with and can help us predict Y . We then “select” the feature that produced the minimum MSE and individually add each other feature to it and repeat the train/test procedure to calculate MSE values. At the end of this round, if the minimum MSE is smaller than the minimum MSE in the previous step, we again select the feature that produced this minimum MSE and repeat the previous procedure. At each step if adding in an additional feature decreases the minimum MSE further, we continue. Otherwise we stop and deem the remaining features as not having much predictive power beyond the “selected” features.

Such feature selection schemes are useful for identifying the halo parameters that are most relevant to inferring N_{gal} .

4. RESULTS

As described in § 2, our tests use a sample of 395,832 halos from the Millennium simulation to assess the machine learning algorithms detailed in the preceding section. We randomly split this halo sample into three equal parts and use the first part for training, the second part for validation and the third part for testing. The base MSE of the test set is ~ 0.505 . We first look at the results obtained through training the ML algorithms on all 6 halo features.

As mentioned in §3.1, we do a grid-search to find the SVM training parameters (C , γ and kernel) that return the minimum MSE on the validation set. This procedure selected the rbf kernel with $C = 1000$ and $\gamma = 0.0001$. We then use the SVM trained using these values to make predictions from the test set. For kNN, we use a similar search technique (described in §3.2) and find that using $k = 12$ gives the minimum MSE on the validation set. The kNN test set results below are derived using this value.

A set of 2D histograms in $N_{gal,true}$ versus $N_{gal,predicted}$ from our test set is shown in Figure 1. The top panel shows the SVM result and the bottom panel shows the kNN result. One can see that in both cases, the MSE

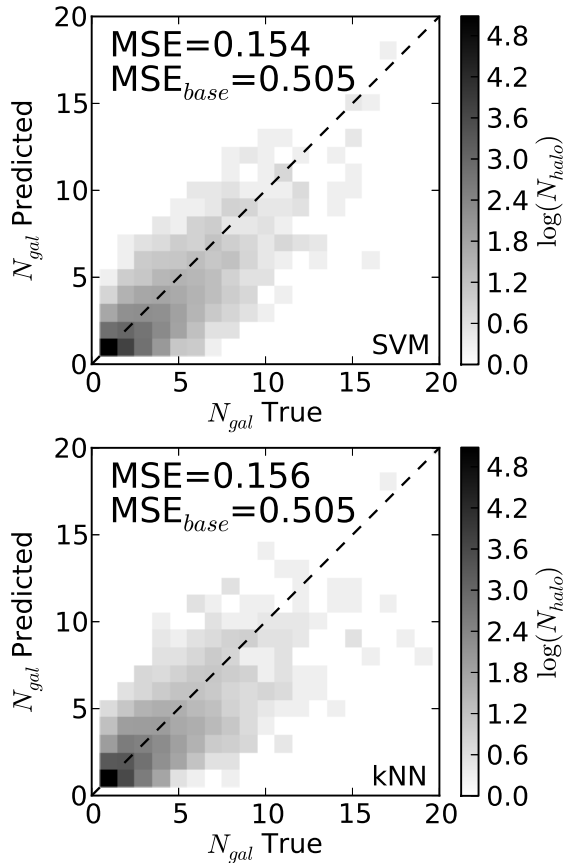


FIG. 1.— 2D histograms of machine-learning-predicted number of galaxies per halo (N_{gal}) versus the true number. Here we have taken the 395,832 halos with $M > 10^{12} h^{-1} M_{\odot}$ from the Millennium simulation and split them randomly and equally into training, validation and test sets. We then use the following features to predict the mapping from halo properties to N_{gal} : number of particles N_p , M_{200} , σ_v , maximum circular velocity v_{max} , half-mass radius $R_{1/2}$ and halo spin. The “goodness” of the prediction is indicated by the MSE (see Equation 1) which is essentially a combined measure of variance and bias. The dashed black line in each panel indicates the 1:1 line. (top) Results from the support vector machine (SVM) algorithm. (bottom) Results from the k-nearest-neighbours (kNN) method. One can see that the MSE is fairly small in both cases. For comparison, the base MSE (the MSE one would obtain if one always predicted N_{gal} to be the average of the training set) is ~ 0.505 , which is a factor of a few larger than the MSE values derived from our ML-predicted N_{gal} . There appears to be a small bias towards under-prediction of N_{gal} ; however this does not seem to detract significantly from our ability to create large-scale structure mocks.

is dramatically improved over the base MSE which indicates that the ML algorithms are learning some information about N_{gal} from the input features as expected. The MSE values from the 2 different methods are very similar and hence SVM and kNN appear to be equally good for inferring N_{gal} from halo features. However, we note that upon careful inspection of the 2D histograms, one sees that there is a slight bias towards under-predicting N_{gal} which is discussed more below.

ML algorithms appear to match the expected distribution of N_{halo} as a function of N_{gal} quite well as shown in Figure 2. The panels show histograms where the y -axes

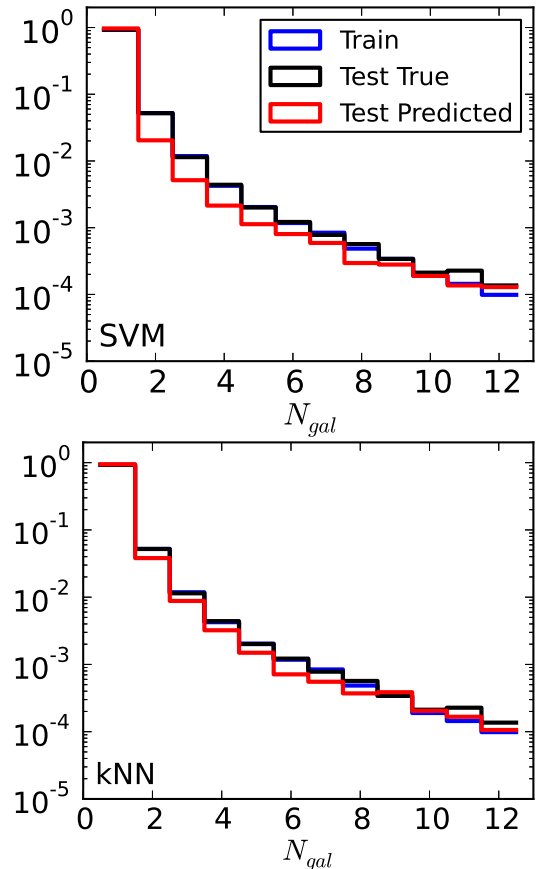


FIG. 2.— Distribution of training, true and predicted test N_{gal} per halo from the Millennium simulation. (top) SVM results. (bottom) kNN results. One can see that the overall distribution of galaxies predicted using the ML algorithms track the true values well. It appears that we slightly overpredict the number of halos with $N_{gal} = 1$ and underpredict elsewhere, however, this does not seem to significantly affect our ability to make mock catalogs for large-scale structure analyses.

correspond to the fraction of halos with N_{gal} and the x -axes correspond to N_{gal} . The top panel was obtained using the SVM method and the bottom panel shows the analogue for kNN. We slightly overpredict the number of halos with 1 galaxy, and underpredict elsewhere, especially when using the SVM. The true number of galaxies in the test set is 149,064; for SVM we predict 140,519 and for kNN we predict 144,346. This phenomenon was pointed out previously and will be elaborated on below.

The galaxy correlation function $\xi(r)$ can also be used to test the robustness of the ML results. This test is especially interesting as $\xi(r)$ is the principal observable for large-scale structure analyses, the key motivation behind constructing mock galaxy catalogs. We create a mock galaxy catalog using the N_{gal} values predicted by our ML algorithms. We place these galaxies randomly within their host halos according to an NFW profile in the radial direction and random point generation on a sphere in the angular directions. We calculate the correlation function for the training, true test set and predicted test set galaxies in $5h^{-1}\text{Mpc}$ bins in the range $5h^{-1}\text{Mpc}$ – $60h^{-1}\text{Mpc}$ (suitable for redshift-space distortion analyses

from large-scale structure). Figure 3 shows the resulting $\xi(r)$ using SVM (top) and kNN (bottom). Each plot has 2 panels, the upper panel shows the actual correlation functions and the bottom panel shows the percent difference (i.e. $100 \times [\xi_{\text{predict}}(r) - \xi_{\text{true}}(r)]/\xi_{\text{true}}(r)$) between the correlation function calculated from the predicted galaxies in the test set versus that calculated from the true galaxies in the test set.

In the SVM case we see that at small scales ($\sim 5h^{-1}\text{Mpc}$), the predicted correlation function has a lower amplitude than the true correlation function by a significant amount ($\sim 40\%$). For kNN, the difference is fairly benign ($\sim 10\%$). At these small scales, the 1-halo term is still important and hence the fact that we underpredict the number of halos with $N_{\text{gal}} > 1$ as shown in Figure 2 will result in lower clustering amplitudes than expected. However, for analyses of large-scale structure, we are more interested in $\xi(r)$ at $r > 30h^{-1}\text{Mpc}$ where our predicted $\xi(r)$ is only $\sim 5 - 10\%$ lower than the true correlation function for the most part. As the amount of underprediction is fairly constant, one can even imagine implementing a simple scaling correction for crude applications. Hence, the potential for making large-scale structure mocks using SVM or kNN remains worthy of further investigation.

As mentioned above, there is a slight bias towards under-predicting N_{gal} . This is likely due to the fact that the number of halos with small N_{gal} dominates the overall distribution while halos with high N_{gal} are much rarer (see Figure 2). Then, taking kNN as an example, even if a halo should have a large number of galaxies, its nearest neighbours may still be dominated by $N_{\text{gal}} = 1$ halos, which will lead the algorithm to underpredict. The current training set is clearly incomplete for halos with large N_{gal} . A larger training sample will have a proportionately larger number of these halos so using a larger training set should be able to partially mitigate this problem. In addition, recall that the best kernel and parameters (C and γ) for the SVM and number of nearest neighbours k for the kNN are selected using the validation set on the basis of minimizing MSE. Since the MSE is a balanced measure of variance and bias, one can imagine giving a different weighting to the bias, i.e. penalizing the MSE more if the bias is high. This can potentially reduce the amount of underprediction we see, however, we will pay the price of having a larger scatter in our predictions.

For SVM we underpredict the total number of galaxies by $\sim 6\%$ and for kNN we underpredict by $\sim 3\%$. These are both small and do not appear to significantly alter the correlation function shown in Figure 3 at scales relevant to large-scale structure analyses. At these scales, the correlation function is dominated by the 2-halo term which comes mostly from halos containing a single galaxy. As discussed above, such halos are the most abundant by far. In addition, Figure 2 indicates that the number of halos we predict with $N_{\text{gal}} = 1$ matches the true distribution reasonably well. Hence, it is not surprising that our predicted $\xi(r)$ is in fair agreement with the true $\xi(r)$ at large r .

We can also look at the distribution of N_{gal} as a function of the various features. Figure 4 shows this in scatter plot form for the kNN test. The analogous plots for SVM are largely the same. Here we have randomly subsampled

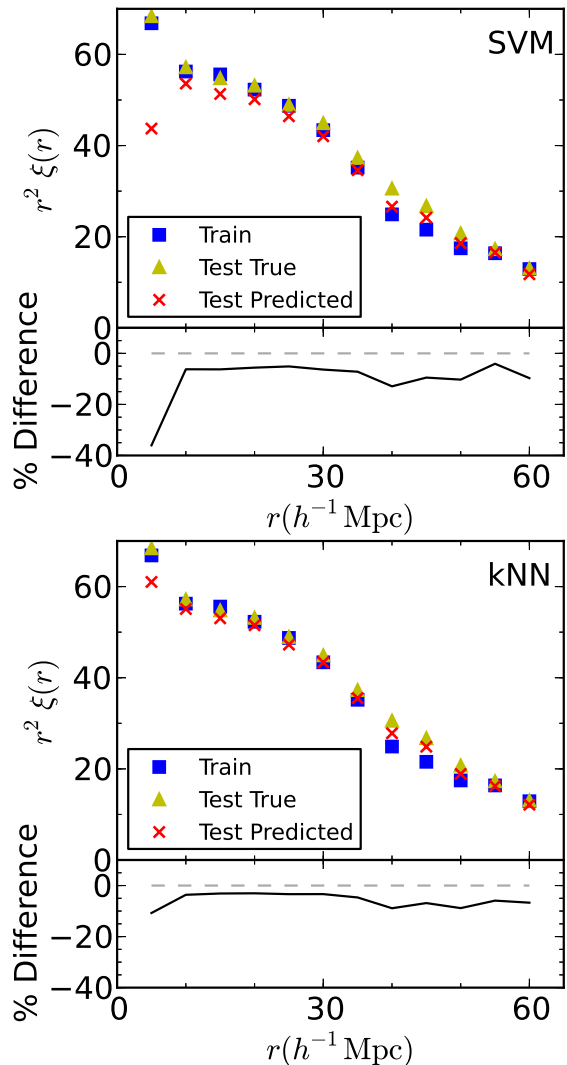


FIG. 3.— Correlation functions $\xi(r)$ of the training, true test and predicted test set galaxies. We create a mock galaxy catalog from the ML-predicted galaxies in order to calculate their $\xi(r)$. This is an excellent test of the ML predictions as $\xi(r)$ is a key observable used for large-scale structure analysis, a major motivator for generating mock galaxy catalogs in the first place. The bottom panels of each plot show the percentage difference between the $\xi(r)$ calculated from the actual test set galaxies and the ML-predictions. The grey dashed line marks 0% to help guide the eye. The correlation functions of the ML-predicted galaxies match the true correlation function well overall. However in the SVM case, due to the underprediction of halos with $N_{\text{gal}} > 1$ at small scales (around $5h^{-1}\text{Mpc}$) where the 1-halo term is still important, the clustering amplitude appears to be 40% smaller than expected. This is not a major deterrent from using ML for making large-scale structure mocks since for these analyses we are mostly interested in scales greater than $\sim 30h^{-1}\text{Mpc}$ where the difference between true and predicted $\xi(r)$ is mostly $< 10\%$. In addition, the kNN case demonstrates better agreement between predicted and true $\xi(r)$ at small scales. Hence, ML provides a potentially interesting alternative for creating large-scale structure mocks.

the number of points plotted to 3,000. The black points show true N_{gal} versus features while the red points show predicted N_{gal} . One can see that overall the span of the points overlaps quite well between the true and predicted sets, again indicating the general statistical agreement between the two. However, the black points do show slightly more spread overall. This indicates that the halo properties we have chosen to use here may not fully encapsulate the mapping to N_{gal} , i.e. we are still missing some information that is relevant to the halo-galaxy relationship. This should not be surprising as most of our parameters (N_p , M_{200} , σ_v , v_{max}) are effectively mass tracers. The ratio of $R_{1/2}$ and R_{200} (calculated easily from M_{200}) can be thought of as a measure of concentration, effectively the ratio of 2 radii that are defined in the same way for all halos. Concentration is known to trace mass (Navarro, Frenk & White 1996), but has also been found to correlate with halo environment (Wechsler et al. 2006; Gao & White 2007; Maccio et al. 2007). One can imagine that in addition to mass, spin and environment, there are additional factors (branching from the full merger history of the halo) that might affect N_{gal} . Fortunately, it appears that any other factors are not completely orthogonal to the halo properties used in this study. As shown above, our parameters seem to capture most of the halo-galaxy mapping, at least in the context of the Millennium simulations.

Finally, we can perform a feature selection to identify, within the framework of Millennium, the most predictive halo property for N_{gal} . We employ a forward feature selection algorithm using SVM to do this. To ensure the stability of our results, we re-perform the feature selection 10 times with different random draws of the training, validation and test sets. Key numbers are summarized in Table 1. The MSE values quoted for each feature under the column heading ‘‘first round’’ correspond to the median MSE values of the 10 trials in the first round of the forward feature selection. One can see that $R_{1/2}$ has the smallest MSE in the first round of selection which indicates that it is the best predictor for N_{gal} . Using $R_{1/2}$ as the only feature for training gives a median MSE of 0.163 which is very close to the MSE obtained using all features as shown in Figure 1. The other parameters yield MSE values ranging from 0.189 (M_{200}) to 0.275 (spin). The values quoted under ‘‘second round’’ correspond to the median MSE obtained by adding in another feature on top of $R_{1/2}$. One can see that this does not significantly change/improve on the minimum MSE from the first round. Hence it appears that most of our constraint on N_{gal} is coming from $R_{1/2}$ in the Millennium simulations. The selection of $R_{1/2}$ should not be surprising. It contains information about the halo mass and, as discussed above, can be related to halo environment through M_{200} .

4.1. Colour-dependent Mocks

The Millennium semi-analytic galaxies come with b , v , r , i , z absolute magnitudes which we can use to define colours and split galaxies into blue and red subpopulations. This allows us to study whether or not ML-based methods for learning the halo-galaxy mapping and, most importantly, making mock catalogs can be directly extended to subpopulations of galaxies that have different

TABLE 1
MSE VALUES OBTAINED BY PERFORMING A FORWARD FEATURE SELECTION USING SVM. THE VALUES QUOTED ARE THE MEDIAN MSE FROM 10 DIFFERENT RANDOMIZATIONS OF THE TRAINING, VALIDATION AND TEST SETS. THE HALO PARAMETERS WE USE ARE LISTED IN COLUMN 1 AND THE MEDIAN MSE VALUES OBTAINED BY USING ONLY THE LISTED PARAMETER ARE SHOWN IN COLUMN 2 (FIRST ROUND). ONE CAN SEE THAT $R_{1/2}$ HAS THE SMALLEST MEDIAN MSE AND HENCE IT SHOULD BE THE BEST PREDICTOR OF N_{gal} IN THE CONTEXT OF THE MILLENNIUM SIMULATIONS. ADDING IN ADDITIONAL PARAMETERS DOES NOT SIGNIFICANTLY CHANGE THE MEDIAN MSE AS INDICATED IN THE THIRD COLUMN (SECOND ROUND) WHICH LISTS THE MEDIAN MSE VALUES OBTAINED USING $R_{1/2}$ PLUS THE PARAMETER LISTED IN COLUMN 1.

Parameter	First Round	Second Round
N_p	0.216	0.170
M_{200}	0.189	0.163
σ_v	0.220	0.163
v_{max}	0.229	0.163
$R_{1/2}$	0.163	–
spin	0.275	0.167

colours. We define blue galaxies to have $(v - r) < 0.7$ and red galaxies to have $(v - r) > 0.7$. This gives 175,177 blue galaxies and 270,792 red galaxies.

We again split the 395,832 halos equally into training, validation and test sets for each case (blue or red) and repeat the previous tests using kNN. Note that many of our halos now have 0 red or blue galaxies reducing the size of our effective training sample. In the case of the blue galaxies, the MSE we obtain after applying kNN is 0.186 as compared to a base MSE of 0.334. For the red galaxies, we obtain an MSE of 0.293 as compared to a base MSE of 0.738. In both cases, there is a significant reduction in MSE compared to the base MSE which indicates that the algorithm is learning information about N_{gal} from our input features.

Correlation functions derived from our predictions are shown in Figure 5. One can see that the predicted $\xi(r)$ agrees fairly well with truth. Again at small scales $\sim 5h^{-1}$ Mpc, we see that the predicted $\xi(r)$ has a lower clustering amplitude, especially for the red galaxies ($\sim 20\%$). If we look at the distribution of halos with N_{gal} , we again see that there is a small under-prediction in the number of halos with $N_{gal} > 1$ that can cause this effect. This is slightly more problematic here as the main goal of studying the dependence of clustering on colour is to understand galaxy formation and evolution mechanisms which rely on information at small scales. However, such problems can be mitigated if we had a larger set of training data. We are now also approaching the point where the number of galaxies observed is large enough for us to begin understanding the differential clustering of blue and red galaxies at large scales. The agreement between the correlation function derived from our ML-predicted galaxies and the true correlation function at these scales is better ($\lesssim 10\%$) and hence ML-based mock catalogs can be useful for these purposes.

4.2. Stellar Mass-dependent Mocks

Since the Millennium semi-analytic galaxy models also supply us with a stellar mass, we can split our galaxies into high stellar mass M_{star} and low stellar mass samples. This can help us understand how effectively we can extend ML-based approaches to understanding the halo-

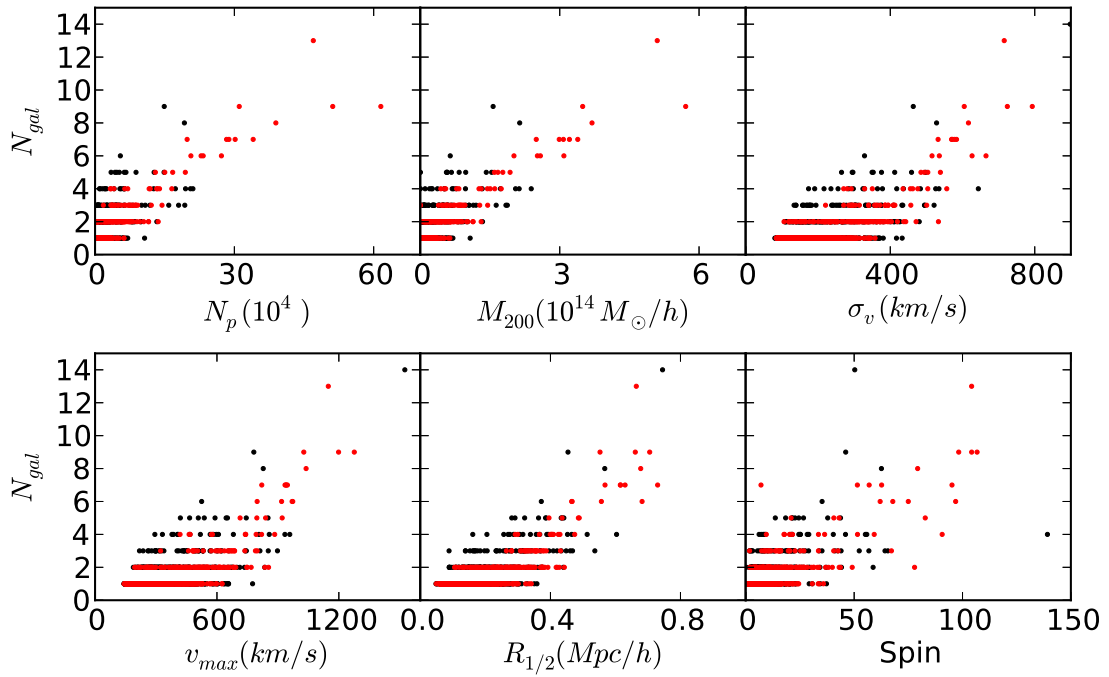


FIG. 4.— Distribution of N_{gal} as a function of the different features. The black datapoints correspond to the true N_{gal} values from the test set and the red datapoints correspond to the ML-predicted values. One can see that the true and predicted points have similar spreads, however, the true points tend to be slightly more spread out overall. This suggests that the features we have used to predict the mapping between halo properties and N_{gal} do not fully capture this relationship, although they do well for the most part. We should not be surprised though as our features mostly trace halo mass and environment. In principle, the full merger history of the halos might impact more than mass and environment. The fact that these 2 key factors already predict the mapping to N_{gal} as well as shown here is impressive.

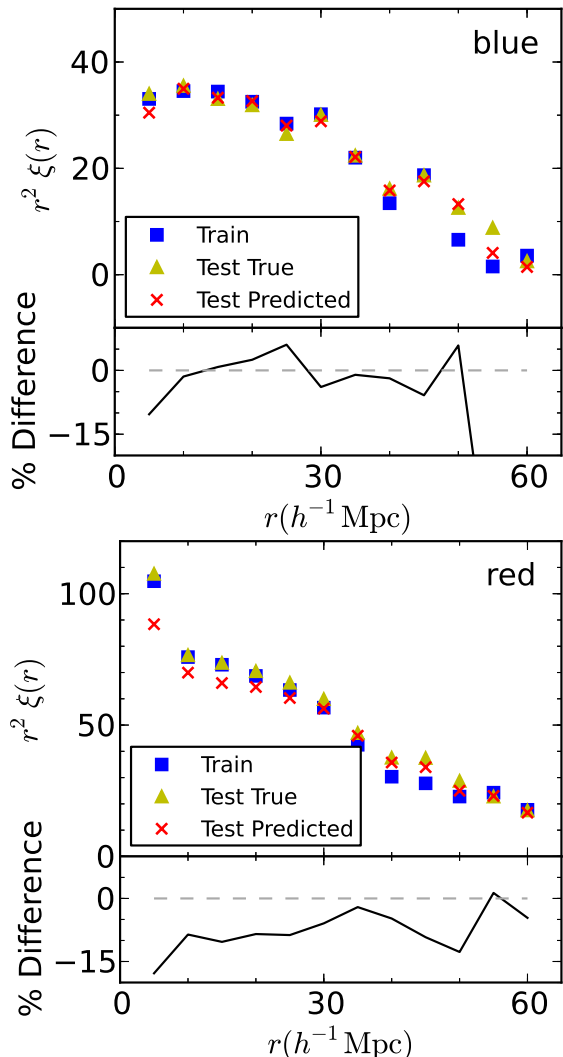


FIG. 5.— Correlation functions of the training, true test set and predicted test set galaxies. Here, we have separated the galaxies into blue and red subpopulations. One can see that the general agreement between predicted and true $\xi(r)$ is not bad with deviations mostly $\lesssim 10\%$. However, there appears to be a slight deficiency in power at small scales, especially for the red galaxies, in the predicted $\xi(r)$. This will make the study of galaxy evolution more problematic since it draws on information contained in the small-scale clustering of galaxies. However, using ML to make color-dependent mocks at large scales remains a possibility.

galaxy mapping as a function of stellar mass, including their potential for constructing mock catalogs for these distinct subpopulations of galaxies. We make the cut at $10^{11} M_{\odot}/h$ which gives 71,573 high M_{star} galaxies and 374,410 low M_{star} galaxies. Stellar mass and luminosity are correlated with each other and hence by performing this split we are effectively separating our galaxies into low and high luminosity samples.

Once again we split the halos randomly and equally into training, validation and test sets. We then run kNN to predict N_{gal} for each of the high and low stellar mass cases. Note that in the high M_{star} case, most of our halos now contain 0 galaxies so we have reduced the effective size of the training set by a large amount here. For the

high mass case, we obtain an MSE of 0.119 after applying kNN as compared to a base MSE of 0.250. For the low mass case, our MSE is 0.214 as compared to a base MSE of 0.283. Again, the MSE after putting the data through a kNN algorithm is smaller than the base MSE, indicating that the algorithm is learning about N_{gal} from the input features.

A plot of the correlation functions derived from the ML-predicted galaxies is shown in Figure 6. The low M_{star} $\xi(r)$ agrees well with truth at large scales ($\lesssim 5\%$ deviation), however, it is again low near $5h^{-1}$ Mpc. Like in the above case where we split by colour, this is slightly troublesome since studying the luminosity dependence of clustering is also mostly focused on understanding galaxy evolution through the clustering at small scales. Nonetheless, mocks produced using our predicted N_{gal} can still benefit studies of luminosity-dependent clustering at large scales. The agreement in the high M_{star} case is poor with deviations $\gtrsim 20\%$. However, this is because there are very few high stellar mass galaxies. With only a small number of halos with non-zero N_{gal} , it is not surprising that the algorithm has some difficulty with the regression. Looking at the overall distribution of halos with N_{gal} in this case reveals an underprediction of halos with $N_{gal} > 0$ (including $N_{gal} = 1$). Having fewer galaxies that break the $N_{gal} = 1$ threshold effectively increases the galaxy bias and hence the clustering amplitude due to the 2-halo term which begins to become important near $\sim 5h^{-1}$ Mpc and is dominant at larger scales.

5. CONCLUSIONS

We have made some preliminary investigations into using machine learning techniques to populate dark matter halos from N-body simulations with galaxies. Since it is very computationally expensive to run cosmological N-body simulations with hydrodynamics, and perturbation theory approaches tend to have problems on small-scales (such as treating redshift-space distortions correctly), machine learning serves as a powerful alternative for creating large numbers of mock galaxy catalogs. These are a key ingredient in large-scale structure analyses, a quickly emerging area with the advent of large galaxy surveys such as LSST, WFIRST and Euclid which will have effective survey volumes of $\sim 10 - 100h^{-3} \text{Gpc}^3$.

Most importantly, machine learning brackets a subclass of non-parametric algorithms which provide a unique way to construct the mapping from halo properties to galaxies. Unlike other techniques such as HOD, we do not need to pre-suppose a known model for the halo-galaxy relationship. The only assumption that must be made is that a function taking halo properties to number of galaxies per halo does exist and that it is smooth. It also allows us to circumvent the problems in subhalo identification which affect SHAM-based approaches.

We test 2 machine learning algorithms, support vector machines and k-nearest-neighbours, on the halos and semi-analytic galaxies in the Millennium simulation. We use 6 halo properties: number of particles N_p , M_{200} , σ_v , maximum circular velocity v_{max} , half-mass radius $R_{1/2}$ and halo spin, to characterize the mapping between halo properties and N_{gal} (the number of galaxies that reside in the halo). We find that both ML algorithms give mean-squared-errors of ~ 0.16 for the predicted N_{gal} , which

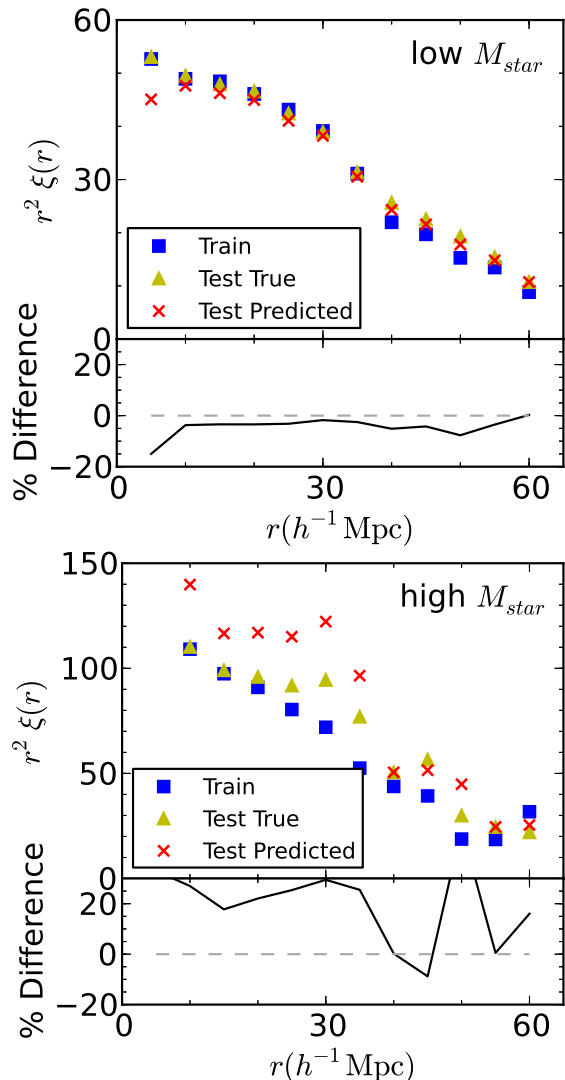


FIG. 6.— Correlation functions of the training, true test set and predicted test set galaxies. Here we have split the galaxies into high and low stellar mass samples. One can see that in the high M_{star} case, the agreement between predicted and true $\xi(r)$ is poor with $\gtrsim 20\%$ differences at most scales. However, this is due to the fact that high stellar mass galaxies are very rare. Most halos do not contain any high M_{star} galaxies which reduces the effective size of our training sample by a large amount. In the low M_{star} case, the predicted and true $\xi(r)$ agree to $\sim 5\%$ at most scales. Again, the slight underprediction of small scale power will make galaxy evolution studies difficult. However, the good agreement at large scales suggests that ML-based approaches for making mock catalogs have potential at these scales.

is much smaller than the base MSE 0.505. The overall distribution of number of halos as a function of N_{gal} is also matched well by the ML predictions. We use our ML-predicted galaxies to create a mock galaxy catalog and calculate the correlation function from it. While in the SVM case we see a deficiency in clustering amplitude at small scales ($\sim 5h^{-1}\text{Mpc}$) by $\sim 40\%$, the predicted correlation function tracks that calculated from the true Millennium galaxies to $\lesssim 10\%$ at the scales most relevant to large-scale structure analyses. This is very important as large-scale structure science is the key motivator be-

hind the construction of mock galaxy catalogs.

Due to the rarity of halos with high N_{gal} , we do find that there is a slight bias towards under-predicting N_{gal} . This can lead to the minor deficit in power at small scales in $\xi(r)$ as mentioned above, however, this does not appear to significantly deter our ability to make mock catalogs. As previously stated, we obtain a reasonably good matching between the predicted and test correlation functions at scales relevant for large-scale structure studies.

We see that the predicted and true N_{gal} values as a function of the features are similar in spread. However, for a given N_{gal} , the spread in the features is slightly larger for the true values. This suggests that the features we have used here do not fully capture the mapping between halo properties and N_{gal} , although, they do come very close. One should not be surprised by this since our features mostly trace halo mass and environment. While key, the full merger history of the halos is likely to impact properties of the halo beyond just mass and environment.

We also demonstrate a simple feature selection procedure on our halo properties. Feature selection is merely the process by which we use machine learning to identify the halo property most predictive in the mapping to N_{gal} . In the context of the Millennium simulations, our feature selection algorithm identifies $R_{1/2}$ as the most relevant parameter. This is not terribly surprising as $R_{1/2}$ is germane to both halo mass and environment.

Finally we investigate direct extensions of our ML algorithms to understanding the halo-galaxy mapping and making mock catalogs for various subpopulations of galaxies (i.e. blue, red, low M_{star} and high M_{star}). We find that in general the agreement between the predicted and true correlation functions is fair. However, once again we observe an underprediction of power at small scales in most cases. As studies of differential clustering in various subpopulations are aimed at understanding galaxy formation and evolution which draw on information contained in the small scales of the correlation function, this is slightly more problematic here. However, we are entering an era where the number of observed galaxies is large enough to engage in studies of differential subpopulation clustering at large scales. Our ML-predicted $\xi(r)$ matches truth to $\sim 5 - 10\%$ at these scales and hence provides an interesting alternative for creating mocks for such studies.

The key advantage of ML is that it offers a method of inferring the halo-galaxy mapping in a model-independent manner. In addition, it is computationally inexpensive: for example, to train an SVM on $\sim 170,000$ points as done in this study takes $\lesssim 1$ hour on a single core. If we can run a large cosmological simulation (N-body plus hydrodynamics) with galaxy formation calibrated against available observations, we should be able to use the ML algorithms tested here to learn the mapping from halo properties to N_{gal} very quickly. We can then create large sets of mock galaxy catalogs from pure N-body simulations which are much less computationally expensive than running a large number of these fully-armed cosmological simulations.

There also exist a number of avenues for future investigation including the use of ML-based approaches to predict not only N_{gal} but also the positions and veloci-

ties of galaxies within the parent halo. This is much more complex as it requires predicting a distribution (i.e. multiple galaxy positions (x, y, z) and velocities (v_x, v_y, v_z)) for each halo. One can also imagine devising methods to mitigate the bias towards underprediction (i.e. penalizing the MSE more for biased predictions or giving more weight to high N_{gal} neighbours in a kNN implementation). These will all aid in our quest to generate mock catalogs reliably and efficiently.

We thank Daniel Eisenstein and Martin White for

helpful discussions. X.X. is supported by a McWilliams Center for Cosmology Postdoctoral Fellowship made possible by the Bruce and Astrid McWilliams Center for Cosmology. H.T. is supported in part by NSF grant AST-1109730. M.N. is supported in part by the M. Hildred Blewett Fellowship of the American Physical Society, www.aps.org. The Millennium Simulation databases used in this paper and the web application providing online access to them were constructed as part of the activities of the German Astrophysical Virtual Observatory.

REFERENCES

- Aizerman, M. A., Braverman, E. M., & Rozonoer, L. I. 1964, *Automation and Remote Control*, 25, 821
- Anderson, L., et al. 2012, *MNRAS*, 427, 3435
- Behroozi, P. S., Wechsler, R. H., Wu, H.-Y., 2011, *ApJ*, submitted [[arXiv:1110.4372]]
- Boser, B. E., Guyon, I. M., & Vapnik, V. N. 1992, A training algorithm for optimal margin classifiers, in Haussler, David (editor), 5th Annual ACM Workshop on COLT, pp. 144, Pittsburgh, PA, ACM Press
- Carlson, J., White, M., & Padmanabhan, N. 2009, *Phys. Rev. D*, 80, id 043531
- Coil, A., et al. 2008, *ApJ*, 672, 153
- Conroy, C., Wechsler, R. H., Kravtsov, A. V. 2007, *ApJ*, 668, 826
- Cortes, C., & Vapnik, V. 1995, *Machine Learning*, 20, 273
- Croft, R. A. C., Di Matteo, T., Khandai, N., Springel, V., Jana, A., Gardner, J. 2012, *MNRAS*, 425, 2766
- Croton, D. J., et al. 2006, *MNRAS*, 367, 864
- De Lucia, G., Springel, V., White, S. D. M., Croton, D., & Kauffmann, G. 2006, *MNRAS*, 366, 499
- De Lucia, G., & Blaizot, J. 2007, *MNRAS*, 375, 2
- Drucker, H., Burges, C. J., Kaufman, L., Smola, A., & Vapnik, V. 1997, *Advances in neural information processing systems*, 155-161
- Gao, L., et al. 2005, *MNRAS*, 363, L66
- Gao, L., & White, S. D. M. 2007, *MNRAS*, 377, L5
- Guo, H., et al. 2012, *ApJ*, submitted, [[arXiv:1212.1211]]
- Lemson, G., et al. 2006, [[arXiv:astro-ph/0608019]]
- Maccio, A. V., Dutton, A. A., van den Bosch, F. C., Moore, B., Potter, D., & Stadel, J. 2007, *MNRAS*, 378, 55
- Manera, M., et al. 2013, *MNRAS*, 428, 1036
- Navarro, J. F., Frenk, C. S., & White, S. D. M. 1996, *ApJ*, 426, 563
- Pedregosa, F., et al. 2011, *JMLR*, 12, 2825
- Springel, V. 2005, *MNRAS*, 364, 1105
- Springel, V., et al. 2005, *Nature*, 435, 629
- Vimal, S., et al., 2010, *MNRAS*, 423, 3458
- Wechsler, R. H., Zentner, A. R., Bullock, J. S., Kravtsov, A. V., & Allgood, B. 2006, *ApJ*, 652, 71
- Zheng, Z., et al. 2009, *ApJ*, 707, 554